Cancer Research

Cancer Stem Cells Regulate Cancer-Associated Fibroblasts via Activation of Hedgehog Signaling in Mammary Gland Tumors

Giovanni Valenti[1], Hazel M. Quinn[1], Guus J.J.E. Heynen[1], Linxiang Lan[1], Jane D. Holland[1], Regina Vogel[1], Annika Wulf-Goldenberg[2], and Walter Birchmeier[1]

Abstract

Many tumors display intracellular heterogeneity with subsets of cancer stem cells (CSC) that sustain tumor growth, recurrence, and therapy resistance. Cancer-associated fibroblasts (CAF) have been shown to support and regulate CSC function. Here, we investigate the interactions between CSCs and CAFs in mammary gland tumors driven by combined activation of Wnt/β-catenin and Hgf/Met signaling in mouse mammary epithelial cells. In this setting, CSCs secrete the Hedgehog ligand SHH, which regulate CAFs via paracrine activation of Hedgehog signaling. CAFs subsequently secrete factors that promote expansion and self-renewal of CSCs. *In vivo* treatment of tumors with the Hedgehog inhibitor vismodegib reduce CAF and CSC expansion, resulting in an overall delay of tumor formation. Our results identify a novel intracellular signaling module that synergistically regulates CAFs and CSCs. Targeting CAFs with Hedgehog inhibitors may offer a novel therapeutic strategy against breast cancer. *Cancer Res; 77(8); 2134–47. ©2017 AACR.*

Introduction

Tumor heterogeneity is believed to be dependent on a distinct subset of tumor cells that possess the capacity to sustain tumor growth, referred to as cancer stem cells (CSC) or tumor-initiating cells (1). CSCs have the ability to self-renew, retaining their features over rounds of cell divisions and to differentiate into multiple cell types, placing them at the top of tumor cell hierarchy. These properties appear to enable CSCs to resist chemotherapy, thereby facilitating relapse (2). CSCs express selective markers at the cell surface and are identified on the basis of their ability to propagate tumors when serially transplanted into recipient mice (3). Tumor cells showing CSC properties have been reported in human and mouse mammary gland tumors (4–7).

CSCs can be regulated by extrinsic signals provided by stromal cells of the tumor microenvironment, which establish favorable conditions for CSC growth (8, 9). Multiple types of stromal cells have been reported to interact with CSCs and to influence their behavior. For instance, endothelial cells provide factors that support CSC proliferation and self-renewal in tumors of the brain and skin (10, 11). Mesenchymal stem cells (MSC) and immune cells establish permissive growing conditions for CSCs in gastric and intestinal tumors (12, 13). In breast cancer, a number of cellular components of the microenvironment have been reported to regulate CSCs, such as MSCs, macrophages, and cancer-associated fibroblasts (CAF; refs. 14–19).

CAFs are major cellular components in the stroma of breast cancers and are involved in many aspects of tumor progression, from the *in situ* growth of primary tumors to the metastatic spread of cancer cells (17–19). The hypothesis has recently been put forward that CSCs and CAFs reside preferentially at the tumor–stroma interface and that both cell types interact with and support each other in a reciprocal fashion (20). CAFs can also cooperate with other stromal cells of the tumor microenvironment, including immune and vascular cells, to establish favorable conditions for tumor growth (21). Recent work has shown that CAFs sustain CSC expansion in colorectal and lung tumors, through the production of secreted factors (22–24). However, the elucidation of this interaction and the identification of supporting factors for CSCs are less well investigated in breast cancer. Here, we unraveled the reciprocal interactions between CSCs and CAFs in our previously described Wnt-Met mouse model of basal-like mammary gland tumors (25).

Materials and Methods

Mouse strains and genotyping

All animal experiments were conducted in accordance with European, National, and MDC regulations. Wnt-Met mice were described previously (25). For genotyping mice, ear punches were digested in lysis buffer (100 mmol/L Tris pH 8.0, 10 mmol/L EDTA, 0.2% SDS, 200 mmol/L NaCl, 300 μg/mL proteinase K) at 55°C overnight. Samples were diluted 1:20 and employed for PCR reactions to amplify transgenes using appropriate set of primers. Products of the amplification were analyzed by agarose (Invitrogen) gel electrophoresis.

[1]Cancer Research Program, Max Delbrueck Center for Molecular Medicine (MDC) in the Helmholtz Society, Berlin, Germany. [2]Experimental Pharmacology & Oncology (EPO), Berlin, Germany.

Note: Supplementary data for this article are available at Cancer Research Online (http://cancerres.aacrjournals.org/).

G. Valenti, H.M. Quinn, and G.J.J.E. Heynen are co-first authors of this article.

Current address for G. Valenti: Department of Digestive and Liver Diseases, Columbia University Medical Center, New York, NY.

Corresponding Author: Walter Birchmeier, Max Delbrueck Center for Molecular Medicine, Robert-Roessle-Str. 10, Berlin 13125, Germany. Phone: 4930-9406-3800; Fax: 4930-9406-2656; E-mail: wbirch@mdc-berlin.de

doi: 10.1158/0008-5472.CAN-15-3490

Histology

Mammary glands were fixed in 4% formaldehyde (Roth) at 4°C overnight and dehydrated in ethanol (Roth). Dehydrated mammary glands were embedded in paraffin and cut into 7-μm sections. Tissue sections were dewaxed, rehydrated, and stained with Hematoxylin (Fluka) and Eosin (Merck). After staining, tissue sections were dehydrated and mounted with Entellan (Merck). Images were acquired using bright-field microscopy (Zeiss).

Immunofluorescence and confocal microscopy

Paraffin-embedded tissue sections were dewaxed and rehydrated. Antigen retrieval was performed to unmask epitopes by boiling sections for 20 minutes in EDTA-Tween buffer (10 mmol/L Tris, 1 mmol/L EDTA, 0.05% Tween-20, pH 9.0). Cryosections were incubated at room temperature for 15 minutes. Adherent cells were fixed in 4% formaldehyde (Roth) at room temperature for 15 minutes. Three-dimensional (3D) structures were fixed in 2% formaldehyde at room temperature for 20 minutes and permeabilized with 0.5% Triton X-100 (Selva) at 4°C for 10 minutes. Samples were incubated with blocking buffer containing 10% goat serum at room temperature for 1 hour. For staining, samples were incubated with primary antibodies at 4°C overnight (see Supplementary Table S1 for the full antibody list). Samples were incubated with secondary antibodies conjugated with Alexa488, Cy3, or Alexa647 (1:400, Jackson ImmunoResearch) at room temperature for 1 hour. Samples were counterstained with 1 mg/mL DAPI solution (1:2,000, Sigma- Aldrich) and mounted with Immu-mount (Thermo Scientific). Pictures were acquired by confocal fluorescence microscopy using a Leica TCS SPE Microscope.

qRT-PCR

Diluted cDNAs were transferred to 96-well PCR optical plates (Thermo Scientific). Selected primers are listed in Supplementary Table S1. SYBR GreenER qPCR mix (Thermo Scientific) was used. qRT-PCR was performed using the iCycler IQTM 5 multicolor real-time detection system (Bio-Rad). Relative mRNA levels were determined following normalization to the housekeeping genes *Actb* or *Rpl19* and analysis with the comparative threshold cycle ($2^{-\Delta\Delta C_t}$) method.

SDS-PAGE and Western blot analysis

Protein samples (30 μg) were incubated at 95°C for 5 minutes in sample buffer (125 mmol/L Tris pH 6.8, 4% SDS, 20% glycerol, 2% β-mercaptoethanol, 0.01% bromophenol blue). Samples were loaded on 8% SDS-PAGE gels (Roth), and proteins were separated using running buffer (25 mmol/L Tris pH 8.6, 192 mmol/L glycine, 0.1% SDS). Samples were transferred on polyvinylidene fluoride membranes (PVDF, Roth) by Mini Trans-Blot (Bio-Rad) in transfer buffer (25 mmol/L Tris pH 8.6, 192 mmol/L glycine, and 20% methanol) at 100 V for 2 hours. Membranes were blocked in 5% nonfat dry milk (Fluka) in TBST (50 mmol/L Tris pH 7.5, 150 mmol/L NaCl, 0.1% Tween-20) at room temperature for 1 hour and incubated with primary antibodies at 4°C overnight. Primary antibodies were goat anti-vimentin (1:100, Santa Cruz Biotechnology), mouse anti-fibronectin (1:1,000, BD Biosciences), and mouse anti-α-tubulin (1:5,000, Sigma-Aldrich). Membranes were developed with Western lightning plus ECL reagent (PerkinElmer) and the Vilber Lourmat imaging system SL-3. α-Tubulin was used as a protein loading control.

Isolation of mammary gland tumor cells

Tumors were minced in DMEM/F12 (Invitrogen) supplemented with 5% FBS (Invitrogen), 5 μg/mL insulin (Sigma-Aldrich), 0.5 μg/mL hydrocortisone (Sigma-Aldrich), 10 ng/mL EGF (Sigma-Aldrich) containing 300 U/mL Collagenase type III (Worthington), and 100 U/mL Hyaluronidase (Worthington) at 37°C for 1-hour shaking. Resulting organoids were resuspended in 0.25% trypsin-EDTA (Invitrogen) at 37°C for 1 minute and digested in dissociation medium–containing 2 mg/mL Dispase (Invitrogen), 0.1 mg/mL DNase I (Worthington) at 37°C for 1-hour shaking. Samples were filtered with 40-μm cell strainers (BD Biosciences) and incubated with 0.8% NH_4Cl solution on ice for 3 minutes (RBC lysis). Cells were labeled with Lineage Cell Depletion Kit (Miltenyi Biotec) and subjected to magnetic-activated cell sorting (MACS).

FACS

Single-cell suspensions were incubated with conjugated primary antibodies at room temperature for 15 minutes (see Supplementary Table S1 for the full antibody list). Cells were next incubated with 7AAD (BioLegend) at room temperature for 5 minutes to stain the DNA of dead cells. Cells were sorted using FACSAria II (BD Biosciences) or analyzed using LSRFortessa (BD Biosciences). Data were analyzed using the FlowJo Analysis Software.

Mammosphere and 3D Matrigel cultures

Single-cell suspensions were plated at 8×10^4 cells/mL in serum-free DMEM/F12 medium, supplemented with 2% B27 (Invitrogen), 20 ng/mL FGF (Invitrogen), 20 ng/mL EGF, 4 μg/mL heparin (Sigma-Aldrich), 5 μg/mL insulin, and 0.5 μg/mL hydrocortisone (mam-medium) for 7 to 14 days on plates coated with 1.2% PolyHEMA (Sigma-Aldrich). Mammosphere cultures were supplemented with mam-medium every 3 days. For coculture experiments, 0.4-μm membrane pore transwell inserts (BD Biosciences) were seeded with CAFs or control fibroblasts (COFs) at 4×10^4 cells/mL in DMEM/F12 containing 1% FBS. Transwell inserts were placed in wells containing single-cell suspensions in mammosphere-forming conditions. Mammospheres were allowed to grow for 7 or 14 days. Numbers and sizes of the mammospheres were determined by phase-contrast microscopy. In experiments involving the use of Wnt-Met reporter mice, fluorescence microscopy was used to detect yellow fluorescent protein (YFP).

For 3D cultures, sorted YFP^+ cells were plated at 1×10^4 cells/well in mam-medium on top of Matrigel layers (BD Biosciences) in 24-well plates and incubated for 14 days. 3D cultures were supplemented with fresh mam-medium every 3 days. For coculture experiments, CAFs or COFs were embedded in Matrigel at 5×10^3 cells/well and incubated at 37°C for 45 minutes to allow the formation of cell–Matrigel layers before seeding CSCs on top.

Cell culture

CAFs were grown in DMEM/F12 supplemented with 10% FBS under standard cell culture conditions. For treatments with recombinant SHH (PreproTech), cells were switched previously to growing medium containing 0.5% FBS. For mammosphere ligand stimulation experiments, cultures were supplemented every 2 to 3 days with mam-medium containing specified

concentrations of the following ligands (R&D Systems): ACTIVIN A (338-AC-010), LIF (8878-LF-025), NOV (1976-NV-050), and IGF-1 (791-MG).

In situ hybridization

Paraffin-embedded tissue sections were dewaxed and rehydrated. Proteins hiding mRNAs were removed by Proteinase K (Roche) treatment. For staining, samples were dehydrated and incubated with DIG-UTP–labeled probes in hybridization buffer in a humidified chamber at 63°C overnight. All buffers and solutions were pretreated with DEPC (1:1,000, Sigma-Aldrich) and autoclaved to inactivate RNases. Samples were incubated first in blocking solution at 4°C for 2 hours and then with anti-DIG Fab fragments coupled with alkaline phosphatase (1:1,000, Roche) at 4°C overnight. Samples were stained with BM-purple (Roche) in the dark at 37°C. Reactions were stopped by washing with PBS. Samples were dehydrated and mounted with Entellan (Merck). Pictures were acquired by bright-field microscopy (Zeiss).

MTT assay

For adherent cultures, cells were seeded at a density of 5×10^3 cells/well in 96-well plates. At determined time points, 20 μL 5 mg/mL 3-(4,5-dimethylthiazol-2-yl)-2,5-diphenyltetrazolium bromide (MTT) solution (Sigma-Aldrich) was added to each well, and cells were further incubated at 37°C for 5 hours. After incubation, growing medium was removed and formazan crystals were dissolved by adding 200 μL DMSO (Sigma-Aldrich). For mammospheres, 200 μL of MTT solution was added to each well of 12-well plates, and cells were further incubated at 37°C for 5 hours. After incubation, mammospheres were collected by gentle centrifugation, resuspended in 200 μL DMSO, and transferred in 96-well plates. Plates were incubated at 37°C for 5 minutes with DMSO before measuring signals at 595 nm using the microplate reader Genios (Tecan).

Microarray and computational analysis

For microarray analysis, RNA was isolated using TRIzol from freshly sorted CAFs, COFs, CSCs, and tumor epithelial cells. RNA samples were cleaned with RNeasy Kit (Qiagen). Quality and purity of RNA samples were assessed by NanoDrop and Bioanalyzer (Agilent) measurements before further processing. RNA (100 ng) was used to synthesize antisense RNAs with the 3′ IVT Express Kit (Affymetrix). Antisense RNAs were hybridized on Mouse Genome 430A 2.0 chips (Affymetrix). Microarray data were analyzed in R statistics using Bioconductor libraries and normalized in RMA with the software BRB-ArrayTools (http://linus.nci.nih.gov/BRB-ArrayTools.html). Microarray data are deposited in the NCBI Gene Expression Omnibus (GEO) with the accession number GSE68241 and accessible at http://www.ncbi.nlm.nih.gov/geo/query/acc.cgi?acc=GSE68241. Genes were functionally annotated using the Database for Annotation, Visualization and Integrated Discovery (DAVID, http://david.abcc.ncifcrf.gov/). Gene set enrichment analysis (GSEA) was performed using default parameters (http://www.broadinstitute.org/gsea/index.jsp). Expression data of tumor stroma from breast cancer patients were retrieved from the Oncomine database (Oncomine, https://www.oncomine.org/).

In vivo pharmacologic treatments

Wnt-Met mice postpartum were administrated orally with vismodegib (50 mg/kg, 100 mg/kg) or control every day, for up to 19 days. Tumor volumes and body weights were determined for each animal several times per week.

For the remaining Materials and Methods, please see Supplementary Information.

Results

CAFs are generated in the stroma of Wnt-Met mammary glands during tumor growth

Histologic analyses of mammary gland tumors generated by combined activation of Wnt/β-catenin and Hgf/Met signaling, as directed by the pregnancy-induced WAP promoter (Wnt-Met mammary gland tumors; ref. 25), revealed significant expansion of the stroma during progression. At 1 week postpartum, the stroma resembled that of control mammary glands with loose fibrotic areas and few fibroblast-like cells (Fig. 1A). At 2 and 3 weeks postpartum, the stroma exhibited massive changes, with increased presence of fibroblast-like cells and extensive extracellular matrix (ECM) deposition. Vimentin, a mesenchymal marker, and smooth muscle actin (SMA), a selective marker for CAFs, were increased after 2 weeks in the stroma surrounding the tumor epithelial compartments, as shown by immunofluorescence (Supplementary Fig. S1A). qRT-PCR and Western blot analysis revealed significant increases in the expressions of vimentin and fibronectin (Fig. 1B and C), an ECM component produced by CAFs (21). These results show that CAF-like structures are generated in the stroma of Wnt-Met mammary gland during tumor growth.

Reciprocal distributions of CSCs and CAFs were assessed by immunofluorescence. CSCs were previously identified in Wnt-Met mammary gland tumors as $CD24^+CD29^{hi}$ and $CD24^+CD49f^{hi}$-expressing cells (25). CD49f showed high selectivity for CSCs by FACS and was employed to analyze CSC distribution. High levels of CD49f were found in tumor epithelial cells positive for keratin 5 (K5) and located in the outermost layers of the tumor epithelial compartments, in close proximity to vimentin-positive CAF-like structures (Fig. 1D). These results suggest mutual interactions exist between CSCs and CAFs in Wnt-Met mammary gland tumors.

A Wnt-Met reporter mouse model, in which activation of WAP-Cre induces constitutive YFP production, was employed to track the fate of recombined cells. As confirmation of transgene activation, YFP^+ cells displayed high protein levels of β-catenin (β-CTN) by immunofluorescence and also high mRNA levels of *Axin2* (a Wnt target gene), *Hgf*, and *Wap* by qRT-PCR (Supplementary Fig. S1B and S1C). YFP was detected in luminal cells of the tumor epithelial compartments at 1 week postpartum, but absent in K14-positive myoepithelial cells (Fig. 1E, Supplementary Fig. S1D). YFP^+ cells expressed E-cadherin but lacked vimentin, K5, and K14, as shown by immunofluorescence. At 2 weeks postpartum, YFP^+ cells kept E-cadherin and low vimentin, but increases of the basal differentiation markers K5 and K14 were observed. qRT-PCR and immunofluorescence on sorted YFP^+ cells confirmed these observations (Fig. 1F and G, Supplementary Fig. S1E).

CD140b and CD90 identify CAFs in Wnt-Met mammary gland tumors

CAFs were isolated from Wnt-Met mammary gland tumors by FACS. A number of cell surface markers were surveyed, and CD140b and CD90 (26, 27) were found to be best suited

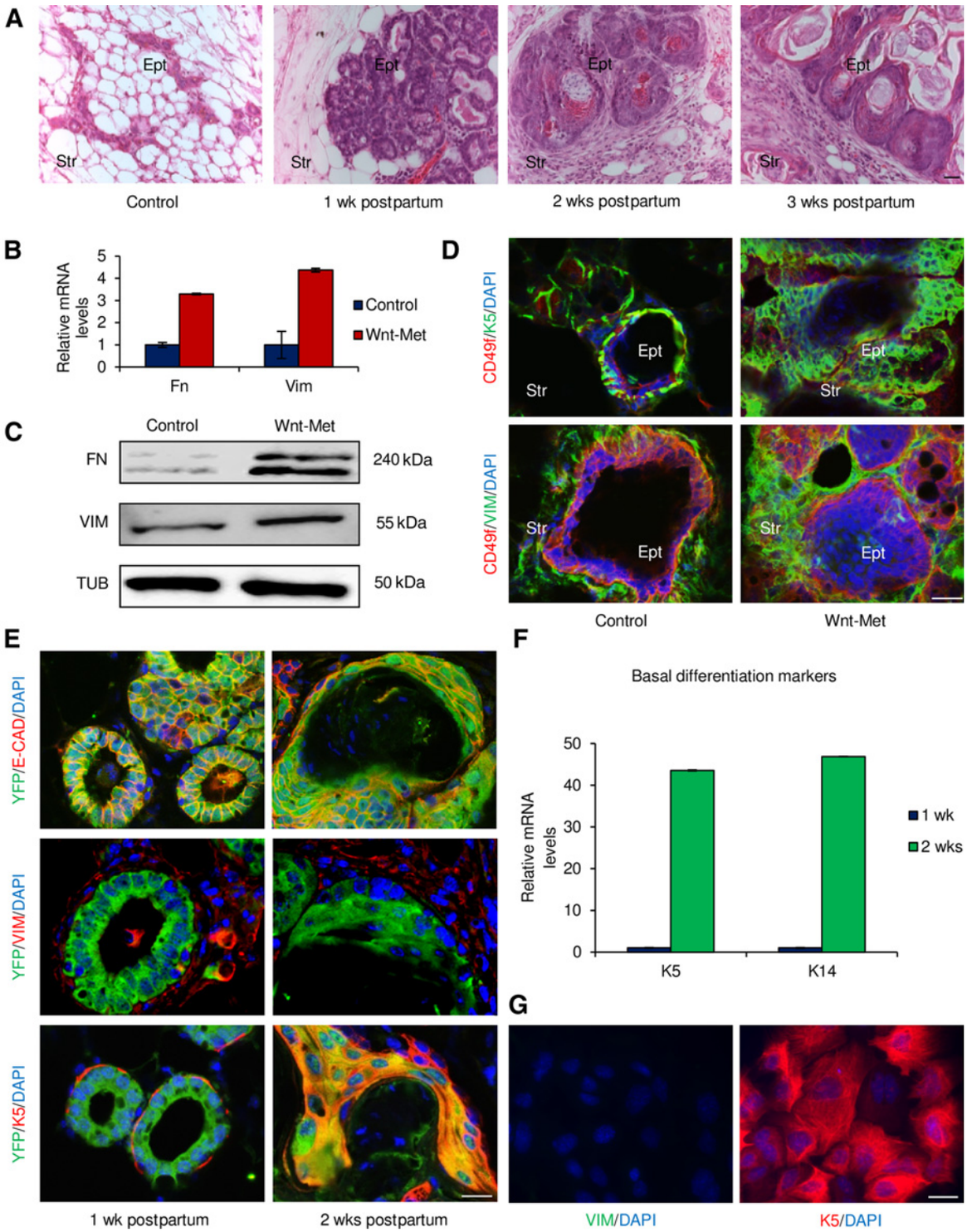

Figure 1.

CAFs are generated in the stroma of Wnt-Met mammary gland tumors. **A,** Hematoxylin and eosin staining of tissue sections from control mammary glands and Wnt-Met tumors at different stages. Ept, epithelium; Str, stroma **B,** qRT-PCR analysis of RNA from control mammary glands and Wnt-Met tumors at 2 weeks postpartum for vimentin and fibronectin. **C,** Western blot analysis of protein lysates from control mammary glands and Wnt-Met tumors at 2 weeks postpartum for vimentin (VIM) and fibronectin (Fn); α-tubulin (TUB) was used as a protein loading control. **D,** Immunofluorescence of tissue sections from control mammary glands and Wnt-Met tumors at 2 weeks postpartum for CD49f, K5, and vimentin. **E,** Immunofluorescence of tissue sections from Wnt-Met reporter mice at different stages for YFP, E-cadherin (E-CAD), vimentin, and K5. **F,** qRT-PCR analysis of RNA from YFP^+ cells sorted from Wnt-Met tumors at 1 and 2 weeks postpartum for basal differentiation markers K5 and K14. **G,** Immunofluorescence of YFP^+ cells sorted from Wnt-Met tumors at 2 weeks postpartum for vimentin and K5. Scale bars, 25 μm.

(Supplementary Fig. S2A and S2B). Immunofluorescence confirmed that CD140b was expressed exclusively in the stromal compartments of Wnt-Met mammary gland tumors (Supplementary Fig. S2C). For sorting, the cell surface marker CD24 was used to exclude epithelial cells. The remaining cells were analyzed for CD140b and CD90. The $CD140b^+CD90^+$ population accounted for 15% to 20% of the parental cells (Fig. 2A). The content of YFP^+ cells in the $CD140b^+CD90^+$ population was negligible (Fig. 2B), confirming the absence of cells of epithelial origin. $CD140b^+CD90^+$ cells displayed high levels of expression of mesenchymal markers (e.g., *Tnc*, *Postn*, etc.; refs. 19, 21), but were negative for epithelial markers (e.g., *K8*, *K14*, etc.; Fig. 2C). Furthermore, these cells did not express any genes associated with transgene activation (*Axin2*, *Hgf*, and *Wap*; Fig. 2D). In culture, $CD140b^+CD90^+$ cells exhibited a spindle cell morphology, protein expression of vimentin and SMA, and the absence of keratin 5 (Fig. 2E; ref. 21). To rule out that the CAFs are not transdifferentiated cancer cells, the recombination status of the β-catenin exon 3 locus in YFP^+ cells and in CAFs was determined by PCR analysis of genomic DNA (Supplementary Fig. S2D). While YFP^+ cells yielded a PCR product, indicating recombination, CAFs did not (Supplementary Fig. S2E). As the cancer cells in this model by definition have undergone recombination, this experiment confirms that CAFs are not derived from cancer cells. These data show that CAFs can be isolated by FACS from Wnt-Met mammary gland tumors. This extended characterization of the CAFs was essential for the subsequent *in vitro* experiments in this work.

CAFs support proliferation, self-renewal, and invasive behavior of CSCs from Wnt-Met mammary gland tumors

To assess potential effects of CAFs on CSC proliferation and self-renewal, a coculture system based on mammosphere formation was employed (Supplementary Fig. S3A; refs. 28, 29). CAFs or COFs were sorted as described above and seeded in transwell inserts with 0.4-μm pore size, which allowed exchange only of soluble factors. Single-cell suspensions from Wnt-Met mammary gland tumors were added into the lower chambers under mammosphere-forming conditions. YFP expression in mammospheres was also examined as a readout for CSC content, as YFP^+ cells were found to be highly enriched within the $CD24^+CD49f^{hi}$ CSC population and also to possess tumor-initiating capacity (Supplementary Fig. S3B; ref. 25). Mammospheres grown for 2 weeks in the presence of CAFs were approximately 2-fold larger than those generated with COFs or without fibroblasts (Fig. 3A–C, top in C). Mammosphere growth measured by the MTT assay indicated that CAFs induced a 2-fold increase in the proliferative capacity of CSCs (Fig. 3C, bottom). In support of CAFs having a positive effect on the proliferation of CSCs, immunofluorescence staining of Wnt-Met tumors showed that CSCs (indicated by nuclear β-catenin) in close proximity to the CAF-enriched (vimentin-positive) stroma exhibited higher expression of the proliferation marker Ki-67 than the other epithelial cells in the bulk of the tumor (Supplementary Fig. S3C). Mammospheres generated in the presence of CAFs also exhibited an approximately 3-fold increase in the content of YFP^+ cells (Fig. 3D–F, top; ref. 25). Dissociated cells from primary mammospheres cultured in the presence of CAFs formed 3-fold more secondary mammospheres than cells previously grown with COFs or without additional cells (Fig. 3F, bottom). These results show that CAFs markedly sustain CSC proliferation and self-renewal.

To evaluate whether CAFs enhanced the invasive behavior of CSCs, a 3D coculture assay was established (Supplementary Fig. S3D; refs. 30, 31). CAFs or COFs were sorted and embedded in Matrigel layers; CSCs were grown in the upper compartments and allowed to generate spheroids. 3D structures generated by CSCs within 2 weeks in culture in the presence of CAFs were significantly larger than those grown with COFs or without fibroblasts (Supplementary Fig. S3E and S3F). 3D structures generated by CSCs grown with COFs or without additional cells were largely round and well organized, with filled lumens. These 3D structures also displayed regular distributions of the polarization markers GM130 (a component of the Golgi complex and apical marker) and laminin (LAM, a component of the basement membrane and basal marker; Fig. 3G, top two panels; refs. 30, 31). However, when grown together with CAFs, CSCs formed aberrant 3D structures characterized by extensive budding and branching. CSCs grown under these conditions failed to generate polarized 3D structures and exhibited aberrant localizations of GM130 and laminin (Fig. 3G, bottom). These observations indicate that CAFs enhance CSCs invasive behavior.

Hedgehog signaling regulates CAFs in Wnt-Met mammary gland tumors

CAFs and COFs were transcriptionally profiled, and a signature was determined of 354 genes, whose expression was 2.5-fold or higher in CAFs in comparison with COFs ($P < 0.001$, FDR < 0.05; Fig. 4A). Functional annotation (32) revealed that the biological categories most significantly represented in the CAF gene signature were indicative of wound healing and inflammatory response, regulation of epithelium and gland development, cell adhesion, and chemotaxis (Fig. 4A; Supplementary Fig. S4A). A number of genes with elevated expression in CAFs compared with COFs in the identified CAF gene signature were validated by qRT-PCR (*Cxcl12*, *Mmp9*, *Spp1*, *Tnc*; Supplementary Fig. S4B). Several genes associated with Hedgehog signaling emerged from the analysis, including *Gli1*, *Ptch1*, and *Ptch2* (Fig. 4A; refs. 33–35). GSEA indicated similarities between the gene signature of CAFs from Wnt-Met mammary gland tumors and reported stromal gene signatures indicative of Hedgehog pathway activation (Fig. 4B; refs. 33, 36). qRT-PCR confirmed the differential expression between CAFs and COFs of genes associated with Hedgehog signaling, including *Gli1*, *Ptch1*, and *Igf1* (Fig. 4C; refs. 33–35). Several genes included in the CAF signature and associated with Hedgehog signaling were also found highly expressed in the stroma of patients with invasive breast cancer ($P < 0.001$; Fig. 4D; refs. 37, 38).

Genes differentially expressed between CAFs and CSCs were also determined by transcriptome analysis of sorted cells (Fig. 4E; refs. 25, 39, 40). A total of 1,139 genes displayed 2.5-fold or higher expression in CAFs than in CSCs ($P < 0.001$, FDR < 0.05; Supplementary Fig. S4C). Functional annotation revealed that genes highly expressed in CAFs were associated with Hedgehog signaling (Supplementary Fig. S4D; refs. 33–35). The differential expression of several Hedgehog target genes between CAFs and CSCs was confirmed by qRT-PCR (Fig. 4F). Genes encoding Hedgehog ligands were not detected in CAFs but in CSCs, which expressed *Shh* (Fig. 4G). The expression of *Shh* and *Ptch1* were further examined by *in situ* hybridization. *Shh* expression could be detected at 1 week postpartum in tumor epithelial cells residing at the tumor–stroma interface (Fig. 4H, left). Increased *Shh* expression was observed in CSCs at the tumor–stroma interfaces

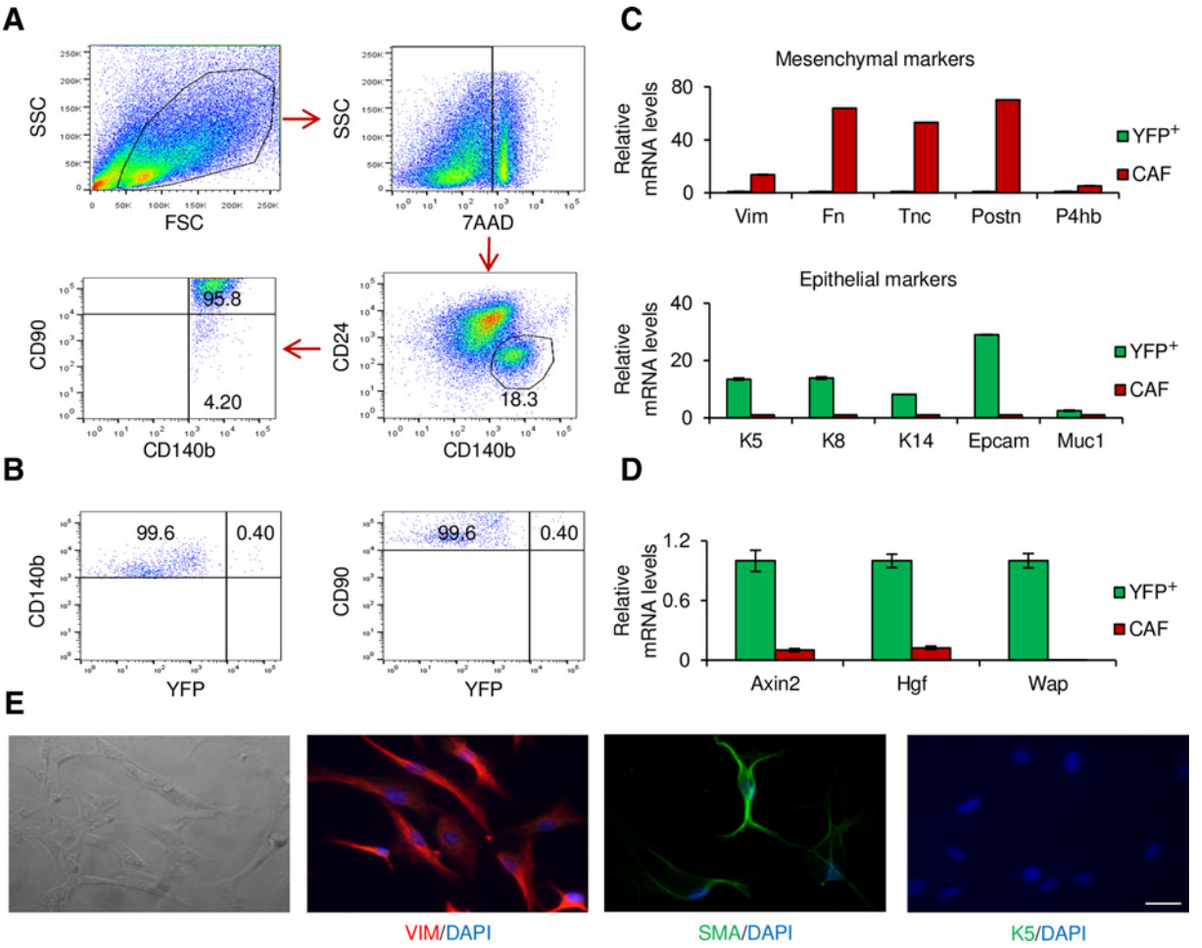

Figure 2.

CD140b$^+$CD90$^+$ cells isolated from Wnt-Met mammary gland tumors exhibit CAF features. **A,** Strategy to isolate CD140b$^+$CD90$^+$ cells by FACS from Wnt-Met tumors. **B,** FACS for YFP of CD140b$^+$CD90$^+$ cells sorted from Wnt-Met tumors. **C,** qRT-PCR analysis of CD140b$^+$CD90$^+$ cells and YFP$^+$ cells sorted from Wnt-Met tumors for mesenchymal (top) and epithelial (bottom) differentiation markers. **D,** qRT-PCR analysis of sorted YFP$^+$ and CD140b$^+$CD90$^+$ cells for genes associated with transgene expression. **E,** Representative bright-field and fluorescence pictures of CD140b$^+$CD90$^+$ cells stained for vimentin (VIM), SMA, and K5. Fn, fibronectin. Scale bars, 25 μm.

from 1 to 2 weeks postpartum. *Ptch1* expression was detected in stromal cells adjacent to the tumor epithelial compartments (Fig. 4H, right). Immunofluorescence confirmed these expression patterns at the protein levels (Supplementary Fig. S4E). CSCs were found to be located at the tumor–stroma interface in the Wnt-Met mammary gland tumors (Fig. 1D). The measurement of the relative distance between CSCs and CAFs revealed that CSCs were approximately 4-fold closer to CAFs with respect to the cells located in the bulk of the tumor mass (Supplementary Fig. S4F). It is known that the diffusive capacity of SHH is very limited, because of its hydrophobic character (41). Thus, SHH potentially produced in the bulk tumor epithelia would not have a significant impact on CAF function. These data indicate that CSC-derived SHH represents the primary source that activates Hedgehog signaling in the neighboring CAFs and suggest that CSCs secrete SHH to stimulate paracrine Hedgehog signaling in closely associated CAFs.

CAFs in culture were then stimulated with recombinant SHH to evaluate potential roles of Hedgehog signaling. Treatments with SHH produced dose-dependent increases in CAF proliferation (Fig. 5A and B; Supplementary Fig. S5A). Increases in mRNA levels of ECM components and CAF differentiation markers were also observed (Fig. 5C). Immunofluorescence also revealed an increase in the protein production of SMA and fibronectin (Fig. 5D and E; Supplementary Fig. S5B and S5C). Moreover, Hedgehog target genes were upregulated in CAFs stimulated with SHH (Fig. 5F). These data show that Hedgehog signaling controls essential aspects of CAF function.

Therapeutic treatment of Wnt-Met mice with a Hedgehog pathway inhibitor reduces tumor stroma and prevents CSC expansion

Wnt-Met mice were systemically treated with vismodegib, an inhibitor of Hedgehog signaling currently approved for the treatment of human patients (42, 43). Treated mice exhibited lower overall tumor volumes (Fig. 6A) with limited signs of toxicity, as indicated by the minimal effects on body weights at 50 mg/kg (Supplementary Fig. S6A). The treatments resulted in histologic

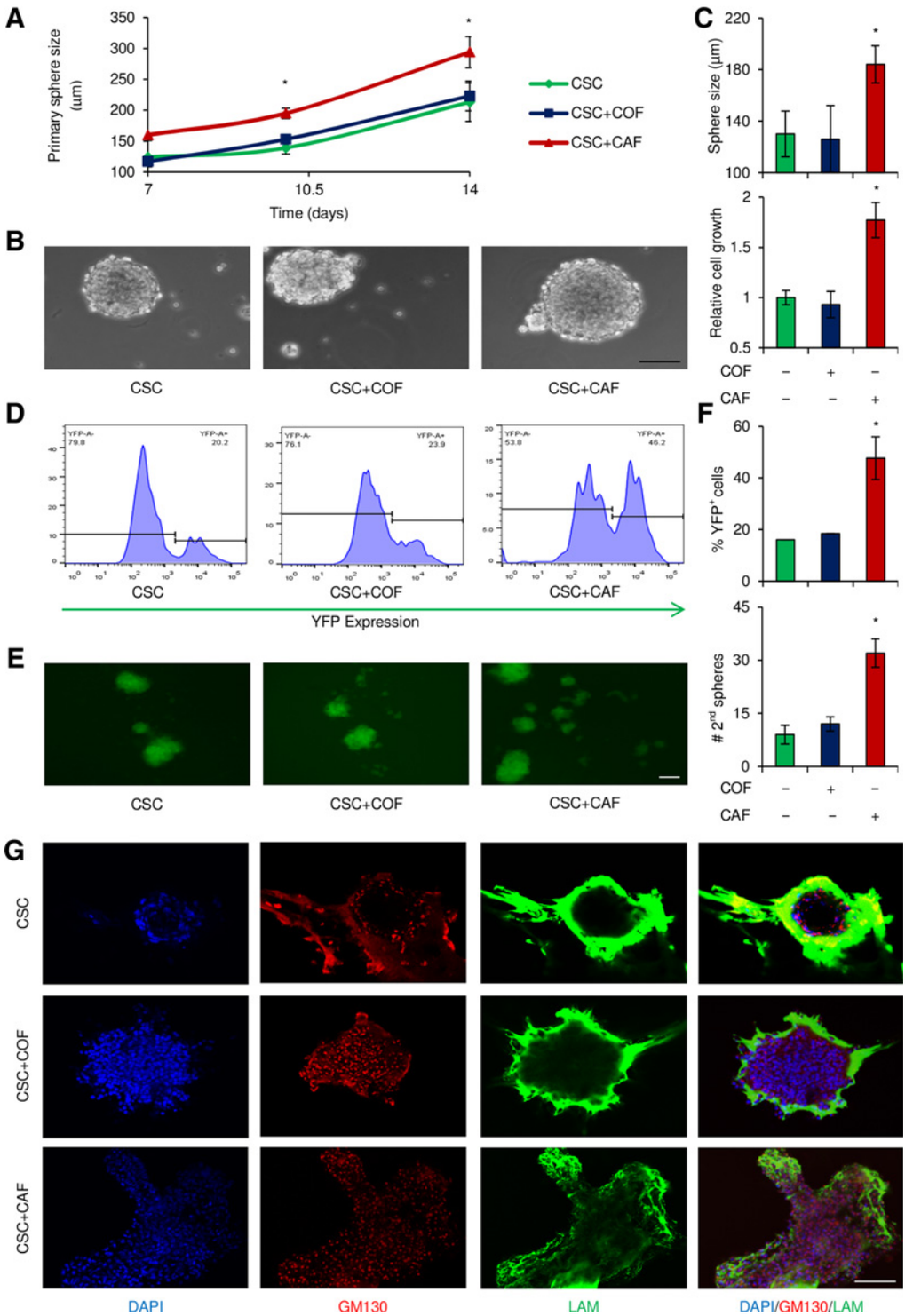

Figure 3.

CAFs promote mammosphere formation and enhance the capacity of CSCs to form invasive 3D structures in Wnt-Met mammary gland tumors. **A,** Size of mammospheres generated alone, with COFs or CAFs over a 2-week culturing period. **B,** Representative bright-field pictures of mammospheres generated alone, with COFs or CAFs after 2 weeks. **C,** Bar charts of average sizes of mammospheres (top) generated alone, with COFs or CAFs, and relative cell growth measured by MTT proliferation assay (bottom). **D,** FACS for YFP in mammospheres generated alone, with COFs or CAFs over a 2-week culturing period. **E,** Representative fluorescence pictures of mammospheres generated alone, with COFs or CAFs. **F,** Bar charts of average percentages of YFP^+ cells in mammospheres (top) generated alone, with COFs or CAFs, and numbers of secondary mammospheres (bottom). **G,** Representative pictures of 3D structures generated alone, with COFs or CAFs over a 2-week culturing period and stained for the polarization markers GM130 and LAM. Scale bars, 100 µm. *, $P > 0.05$.

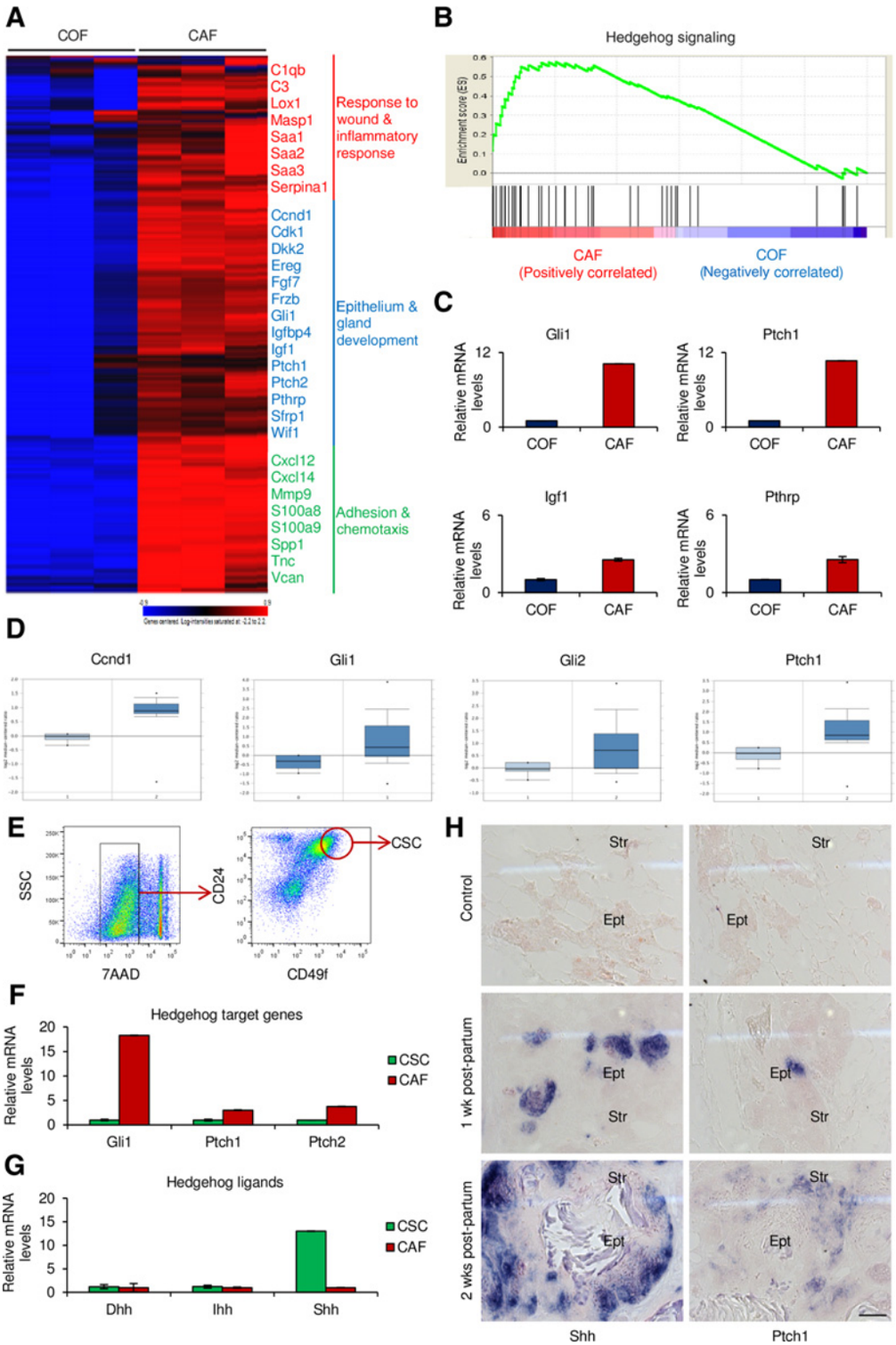

Figure 4.

CAFs from Wnt-Met mammary gland tumors display activation of Hedgehog signaling. **A,** Heatmap of gene expression and gene grouping comparing COFs and CAFs. **B,** GSEA of the gene expression profiles of CAFs and COFs for Hedgehog signaling. **C,** qRT-PCR analysis of CAFs and COFs for Hedgehog pathway genes (top) and genes regulated by Hedgehog signaling (bottom). **D,** Expression of Hedgehog genes in the stroma of breast cancer patients. Left, normal stroma; right, tumor stroma. **E,** Strategy employed to isolate CSCs by FACS from Wnt-Met tumors. **F,** qRT-PCR analysis of CSCs and CAFs sorted from Wnt-Met tumors for Hedgehog pathway genes. **G,** qRT-PCR analysis of CSCs and CAFs sorted from Wnt-Met tumors for Hedgehog ligands. **H,** *In situ* hybridization of tissue sections from control mammary glands and Wnt-Met tumors at 1 and 2 weeks postpartum for *Shh* and *Ptch1*. Scale bar, 25 μm.

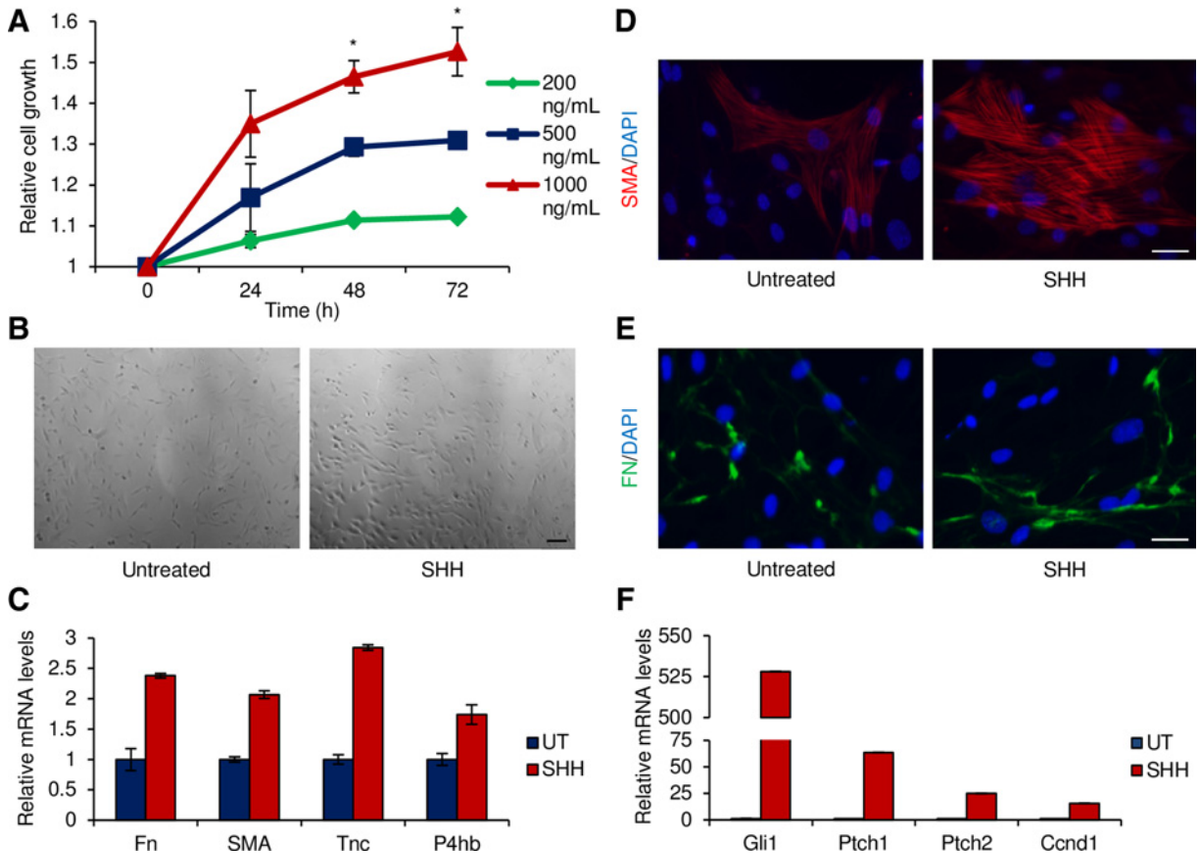

Figure 5.

Hedgehog signaling regulates CAFs in Wnt-Met mammary gland tumors. **A,** Relative cell growth of CAFs stimulated with increasing concentrations of SHH for 24, 48, and 72 hours, as measured by MTT assay. *, $P > 0.05$. **B,** Representative bright-field pictures of CAFs stimulated with SHH for 48 hours. **C,** qRT-PCR analysis of CAFs stimulated with SHH for ECM components and CAF differentiation markers. Fibronectin, Fn. **D,** Representative fluorescence pictures of CAFs stimulated with SHH and stained for SMA. **E,** Representative fluorescence pictures of CAFs stimulated with SHH and stained for fibronectin. **F,** qRT-PCR analysis of CAFs stimulated with SHH for Hedgehog target genes. UT, untreated. Scale bars, 25 μm.

changes in the tumors, which exhibited multiple areas of loose stroma and normal alveolar structures (Fig. 6B). Significant reduction in SMA was observed in the stroma of treated mice, as seen by immunofluorescence (Fig. 6C). Ki-67 staining of vismodegib-treated tumors showed a reduction in proliferation of both stromal and epithelial cells (Fig. 6D; Supplementary Fig. S6B and S6C). CAFs from treated mice also showed significant reductions in their proliferation in culture (Supplementary Fig. S6D). CAFs also exhibited reduced expression of ECM components and CAF differentiation markers (Fig. 6E). Many Hedgehog pathway components and target genes were strongly downregulated in CAFs from treated mice (Fig. 6F). These results show that the inhibition of Hedgehog signaling prevents CAF expansion from mammary gland tumors.

CSCs were analyzed to evaluate whether inhibition of Hedgehog signaling could also affect their biological behavior. FACS revealed reductions in the fractions of YFP^+ cells in mammary gland tumors from mice treated with vismodegib (Supplementary Fig. S6E). Tumor cells from treated mice formed fewer primary mammospheres in culture, which also showed considerable reductions in their average sizes (Fig. 6G and H; Supplementary Fig. S6F). Furthermore, vismodegib treatments strongly inhibited the capacity of CSCs to generate 3D structures in culture, which were significantly smaller, largely rounded, and with filled lumens (Fig. 6I and J; Supplementary Fig. S6G). The mammosphere sizes of CSCs treated *in vitro* with increasing concentrations of vismodegib were not affected after 2 weeks of growth (Supplementary Fig. S6H), but the number of mammospheres formed by CSCs treated with high concentrations of vismodegib after 2 weeks of growth were significantly decreased, suggesting an effect on primary mammosphere formation (Supplementary Fig. S6I). These data suggest that the inhibition of Hedgehog signaling depletes CAFs from tumors and exerts major effects on CSC function, resulting in tumor inhibition.

Hedgehog signaling regulates the production of CAF ligands involved in the regulation of CSCs in Wnt-Met mammary gland tumors

The CAF gene signature was highly enriched for genes encoding secreted proteins (Fig. 4A), suggesting that these cells may interact with CSCs through the production of secreted factors. To identify these factors, a signature of genes highly expressed by CSCs with respect to the cells in the bulk of the tumor mass was determined

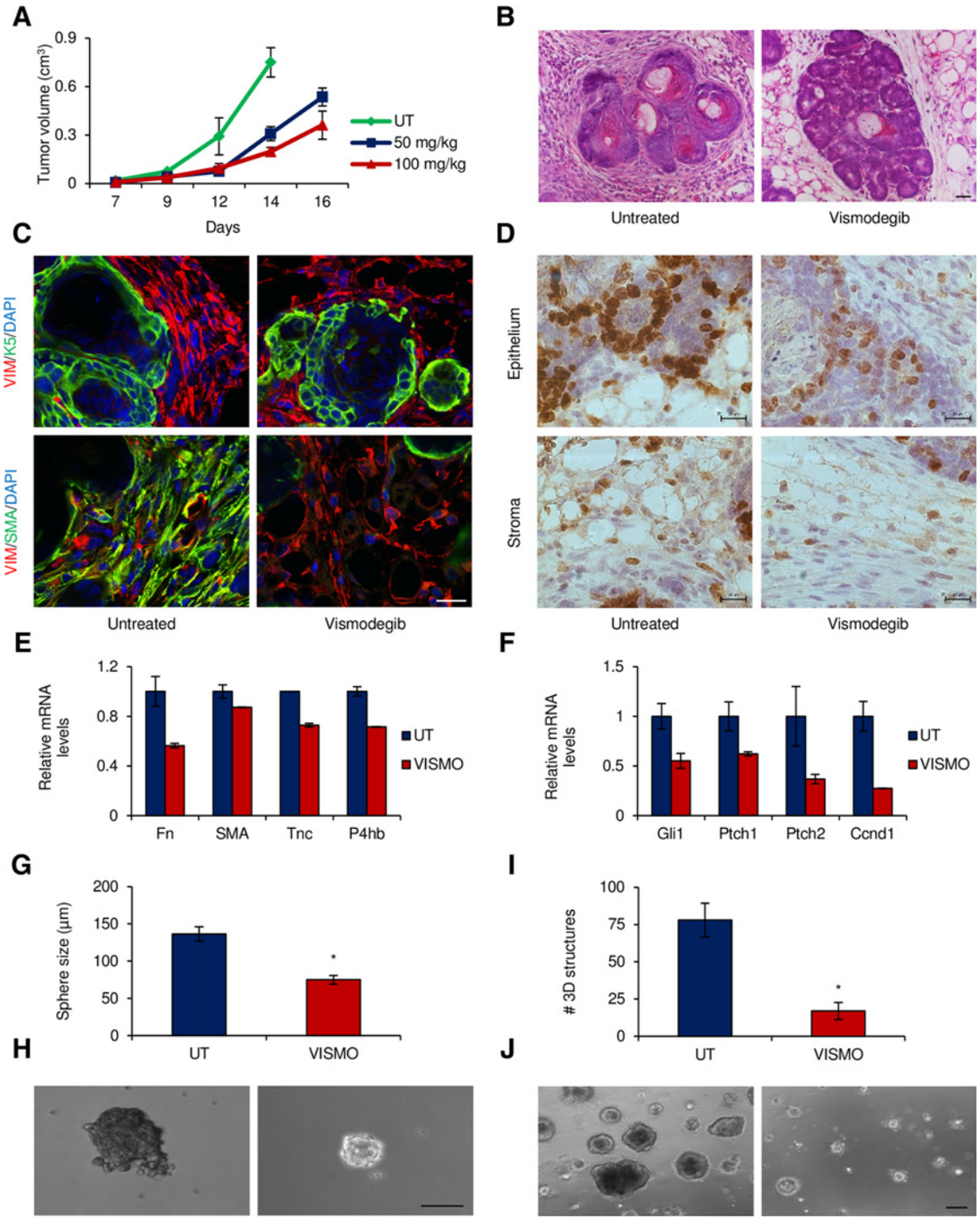

Figure 6.

Therapeutic treatment of Wnt-Met mice with a Hedgehog pathway inhibitor depletes tumor stroma and prevents CSC expansion. **A,** Volume of mammary gland tumors from Wnt-Met mice treated with increasing concentrations of vismodegib over 16 days. **B,** Hematoxylin and eosin staining of tissue sections from untreated and vismodegib-treated Wnt-Met tumors. **C,** Immunofluorescence of tissue sections from untreated and vismodegib-treated Wnt-Met tumors for vimentin (VIM), SMA, and K5. Scale bar, 25 µm. **D,** Ki-67 staining of epithelial and stromal compartments of untreated and vismodegib-treated Wnt-Met tumors. **E,** qRT-PCR analysis of CAFs sorted from untreated and vismodegib-treated Wnt-Met tumors for ECM components and CAF differentiation markers. VISMO, vismodegib. **F,** qRT-PCR analysis of CAFs sorted from untreated and vismodegib-treated Wnt-Met tumors for Hedgehog target genes. **G,** Bar chart of average sizes of mammospheres generated by single-cell suspensions from untreated and vismodegib-treated Wnt-Met tumors. **H,** Representative bright-field pictures of mammospheres generated by single-cell suspensions from untreated and vismodegib-treated Wnt-Met tumors. **I,** Bar chart of average numbers of 3D structures generated by CSCs sorted from untreated and vismodegib-treated Wnt-Met tumors. **J,** Representative bright-field pictures of 3D structures generated by CSCs sorted from untreated and vismodegib-treated Wnt-Met tumors. Scale bar, 100 µm. *, $P > 0.05$.

by transcriptome analysis (Supplementary Fig. S7A; refs. 39, 40). A total of 852 genes were upregulated with a 2.5-fold change or higher in CSCs ($CD24^{+}CD49f^{hi}$) in comparison with $CD24^{+}CD49f^{lo}$ cells that form the bulk of the tumor mass ($P < 0.001$, FDR < 0.05). The CSC gene signature was highly enriched for genes involved in cell adhesion, epithelium and gland development, and receptor signaling (Supplementary Fig. S7A). qRT-PCR confirmed the increased expression of several genes by CSCs (Supplementary Fig. S7B).

One way that CAFs could potentially influence CSCs is via secretion of ligands/growth factors. To identify ligands that could be involved in the CAF–CSC interaction, the transcriptome analyses from Fig. 4A and Supplementary Fig. S7A were evaluated. The CAF gene signature was filtered for genes encoding extracellular proteins, using information from the public database Uniprot (http://www.uniprot.org). Ligands expressed by CSCs or with weak expression in CAFs were filtered out. The remaining candidate ligands were screened for corresponding receptors in the CSC gene signature, using the public databases Uniprot and STRING (http://string-db.org). Multiple CAF ligand–CSC receptor pairs emerged from the analysis (Supplementary Table S2). To validate the expression of a number of the identified ligands, the expression of these ligands was measured in FACS-sorted CAFs and YFP^{+} cancer cells by qRT-PCR. Indeed, all the ligands measured were highly expressed in CAFs in comparison with the cancer cells (Supplementary Fig. S7C). Six of the identified ligands were also found to be highly expressed in the stroma of patients with invasive breast cancer ($P < 0.001$; Supplementary Fig. S7D). Several of these CAF ligands showed reduced expression in CAFs from Wnt-Met mice treated with vismodegib (Fig. 7A), but were increased upon *in vitro* SHH treatment (Fig. 7B), suggesting that Hedgehog signaling could regulate their expression.

Four of the identified CAF ligands were tested in the mammosphere assay to confirm their effects on CSC functions and specifically on proliferation and self-renewal. Mammospheres grown from single-cell suspensions treated with the ligands ACTIVIN A and NOV were significantly increased in size after 1 week (Fig. 7C). IGF-1 and LIF also displayed a trend toward increased mammosphere size. The number of primary mammospheres generated in the presence of the ligands showed the same trends as the mammosphere size (Supplementary Fig. S7E). Fluorescence microscopy confirmed the expansion of the initially seeded YFP cell population after 1 week of growing mammospheres in the presence of the ligands (Fig. 7D). These data indicate that these ligands produce an effect on CSC proliferation. The number of secondary mammospheres formed by single-cell suspensions treated with ACTIVIN A was increased, pointing to an additional role in self-renewal for ACTIVIN A (Fig. 7E). These results show that activation of Hedgehog signaling in CAFs stimulates the secretion of ligands that operate in a paracrine manner on CSCs, regulating their proliferation and self-renewal.

Discussion

In this study, we show that SHH is produced by CSCs in Wnt-Met mammary gland tumors and that SHH induces the expression of target genes of Hedgehog signaling in CAFs, resulting in increased proliferation and ECM deposition. In response to Hedgehog activation, CAFs also produce ligands such as ACTIVIN A, NOV, IGF-1, LIF, and others, which establish permissive conditions for CSC growth, that is, increased mammosphere size and self-renewal. Our data thus identify a new synergistic network between CSCs and CAFs. In previous mammary gland and breast cancer studies, data on reciprocal signaling between CSCs and CAFs have rarely been investigated in such complexity as in the current work. However, as our study mainly focuses on a transgenic mouse model, further investigation in human breast cancer tissue to confirm a similar mechanism is necessary.

In mammary glands, mutations of Hedgehog pathway components in epithelial cells rarely correlate with tumor onset (34, 44). Hedgehog signaling may thus be relevant in particular for the regulation of the stroma adjacent to the epithelia in mammary gland tumors, as also reported in pancreatic tumors (34, 45, 46). A previous study has reported that human breast cancers exhibit Hedgehog pathway activation primarily in the tumor stroma (47). High SHH ligand in the epithelial compartment and high GLI1 in the stroma have been correlated to the increased risk of metastasis and to the reduced survival in a large human cohort of basal breast cancers and in a mouse model (47). Stromal activation of Hedgehog signaling has also been observed in the MMTV-Wnt1 mouse model of mammary gland tumors, which displays expansions of CSC populations (5, 48). These observations suggest that stromal Hedgehog signaling may be important in terms of CSC regulation in mammary gland tumors. We have shown that CSCs are located close to the tumor–stroma interface and produce significant levels of SHH. In contrast, Hedgehog signaling is active primarily in CAFs, despite these cells not producing Hedgehog ligands. The findings we present here suggest a model in which CSCs use Hedgehog signaling to educate CAFs to support their growth by providing factors required for their maintenance. These factors appear to be important in terms of CSC regulation in mammary gland tumors.

We found that CAFs promote the proliferative and self-renewal capacities of CSCs, as seen by an increase of mammospheres grown in the presence of CAFs. The supportive role of CAFs on CSC self-renewal has been previously observed in experiments involving the use of human breast cancer cell lines (19, 49). In other tumors, CAFs have been reported to promote CSC expansion through alternative mechanisms, for instance, CAFs stimulating the acquisition of CSC properties in differentiated tumor cells by inducing EMT (22). In lung cancer, CAFs induced the dedifferentiation of committed tumor cells by activating the expression of genes associated with stemness (24). Here, we present data supporting a novel mechanism by which CAFs influence the function of CSCs through the production of secreted factors, in response to the activation of Hedgehog signaling. We identified several ligands provided by CAFs that could potentially support CSC function. For instance, we identified ACTIVIN A as a potent regulator of CSC proliferation and self-renewal in mammospheres. It would be therefore interesting to further elucidate how ACTIVIN A affects CSC proliferation and self-renewal.

We also found that CAFs alter the invasive behavior of mammary gland CSCs. CSCs grown together with CAFs form aberrant 3D structures, characterized by irregular acini, filled lumens, and dysregulated epithelial polarity. Previous observations obtained in cotransplantation studies reported roles for CAFs in the formation of highly invasive breast cancers (18). Our *in vitro* data suggest that CAFs promote the transition of tumors to invasive phenotypes through selective effects on CSCs. Recent studies have shown that subsets of highly invasive CSCs reside at the

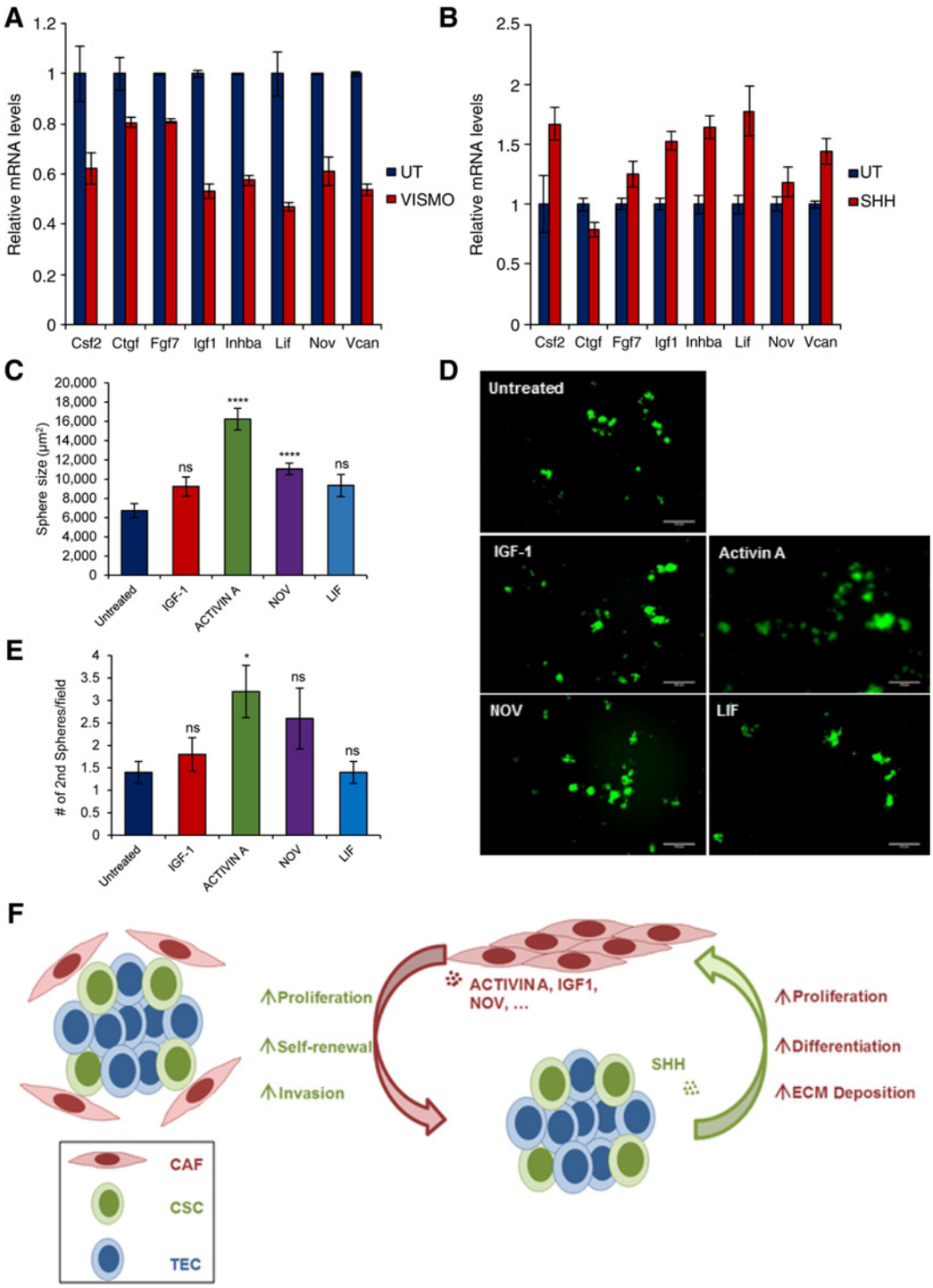

Figure 7.

Hedgehog signaling regulates the production of CAF ligands involved in the regulation of CSCs in Wnt-Met mammary gland tumors. **A,** qRT-PCR analysis of CAFs sorted from untreated and vismodegib-treated Wnt-Met tumors for CAF ligands potentially involved in CSC regulation. **B,** qRT-PCR analysis of CAFs stimulated with SHH for vismodegib-regulated ligands. **C,** Mammosphere sizes of untreated single-cell suspensions and single-cell suspensions treated with IGF-1 (100 nmol/L), ACTIVIN A (10 nmol/L), NOV (50 nmol/L), and LIF (1 nmol/L) after 1 week of growth. Data points, mean ± SEM. ns, not significant. ****, $P < 0.0001$ (one-way ANOVA). **D,** Fluorescence microscopy on YFP$^+$ cells in mammospheres grown for 1 week from untreated single-cell suspensions and single-cell suspensions treated with IGF-1 (100 nmol/L), ACTIVIN A (10 nmol/L), NOV (50 nmol/L), and LIF (1 nmol/L). Scale bar, 200 μm. **E,** Number of secondary (2nd) mammospheres untreated or grown for 1 week in the presence of IGF-1 (100 nmol/L), ACTIVIN A (10 nmol/L), NOV (50 nmol/L), and LIF (1 nmol/L). *, $P > 0.05$. **F,** Scheme of CSC niche (left) and interaction networks between CAFs and CSCs (right) in Wnt-Met tumors. TEC, bulk tumor epithelial cells.

tumor–stroma interfaces in pancreatic cancers (50). It is possible that the acquisition of invasive properties by CSCs depends on factors provided by CAFs. However, further investigation is required to validate the effect of CAFs on CSC invasion *in vivo*.

Targeting the ability of CSCs to create a supportive microenvironment may allow the development of novel therapeutic strategies. This approach has been employed successfully in brain tumors in mice, where blocking the formation of the tumor vasculature resulted in reduced CSC content and arrest of tumor growth (10). We found that treatment of Wnt-Met mice with the Hedgehog inhibitor vismodegib caused a delay in tumor formation. Treated tumors exhibited a reduction of the tumor stroma, which showed reduced presence of CAFs and less fibrotic areas. Treated tumors also displayed significant reduction in the CSC content, as indicated by the impaired capacities of isolated tumor cells to generate mammospheres and 3D structures. The inhibition of Hedgehog signaling may deplete CSCs due to a lack of the factors provided by CAFs, which are required for their maintenance.

In conclusion, the data presented here demonstrate that in Wnt-Met mammary gland tumors, CSCs actively participate in the formation of a supportive microenvironment. CSCs secrete Sonic Hedgehog, which stimulates paracrine activation of Hedgehog signaling in CAFs (Fig. 7F). As a result, CAFs produce soluble factors such as ACTIVIN A, IGF-1, and LIF, which promote CSC proliferation, self-renewal, and potentially invasive behavior. The treatment of mice with a Hedgehog inhibitor caused significant delays in tumor formation, reduction of tumor stroma, and reduced CSC content. Our study may therefore pave the way for treatments based on targeting interactions between CAFs and CSCs as a potential therapeutic strategy against breast cancers.

Disclosure of Potential Conflicts of Interest

No potential conflicts of interest were disclosed.

Authors' Contributions

Conception and design: G. Valenti, J.D. Holland, W. Birchmeier
Development of methodology: G. Valenti, L. Lan
Acquisition of data (provided animals, acquired and managed patients, provided facilities, etc.): G. Valenti, H.M. Quinn, G.J.J.E. Heynen, A. Wulf-Goldenberg, W. Birchmeier
Analysis and interpretation of data (e.g., statistical analysis, biostatistics, computational analysis): G. Valenti, H.M. Quinn, G.J.J.E. Heynen, L. Lan, J.D. Holland, W. Birchmeier
Writing, review, and/or revision of the manuscript: G. Valenti, H.M. Quinn, G.J.J.E. Heynen, J.D. Holland, W. Birchmeier
Administrative, technical, or material support (i.e., reporting or organizing data, constructing databases): R. Vogel
Study supervision: J.D. Holland, W. Birchmeier

Acknowledgments

We thank Dr. Hans-Peter Rahn and the FACS Core Facility at the MDC for the expertise with cell sorting, Dr. Anje Sporbert and the Confocal Microscopy Core Facility at the MDC for support with microscopy. We also thank Dr. Annabel Christ of the MDC for providing reagents to study Hedgehog signaling and Russel Hodge from the MDC for helpful discussions and improvements in the manuscript.

Grant Support

G. Valenti was a recipient and H.M. Quinn is presently a recipient of the International PhD fellowship of the MDC and the Humboldt University of Berlin.

The costs of publication of this article were defrayed in part by the payment of page charges. This article must therefore be hereby marked *advertisement* in accordance with 18 U.S.C. Section 1734 solely to indicate this fact.

Received December 30, 2015; revised January 2, 2017; accepted January 19, 2017; published OnlineFirst February 15, 2017.

References

1. Kreso A, Dick JE. Evolution of the cancer stem cell model. Cell Stem Cell 2014;14:275–91.
2. Dean M, Fojo T, Bates S. Tumour stem cells and drug resistance. Nat Rev Cancer 2005;5:275–84.
3. Visvader JE, Lindeman GJ. Cancer stem cells in solid tumours: accumulating evidence and unresolved questions. Nat Rev Cancer 2008;8:755–68.
4. Al-Hajj M, Wicha MS, Benito-Hernandez A, Morrison SJ, Clarke MF. Prospective identification of tumorigenic breast cancer cells. Proc Natl Acad Sci U S A 2003;100:3983–8.
5. Vaillant F, Asselin-Labat ML, Shackleton M, Forrest NC, Lindeman GJ, Visvader JE. The mammary progenitor marker CD61/beta3 integrin identifies cancer stem cells in mouse models of mammary tumorigenesis. Cancer Res 2008;68:7711–7.
6. Zhang M, Behbod F, Atkinson RL, Landis MD, Kittrell F, Edwards D, et al. Identification of tumor-initiating cells in a p53-null mouse model of breast cancer. Cancer Res 2008;68:4674–82.
7. Holland JD, Klaus A, Garratt AN, Birchmeier W. Wnt signaling in stem and cancer stem cells. Curr Opin Cell Biol 2013;25:254–64.
8. Barcellos-Hoff MH, Lyden D, Wang TC. The evolution of the cancer niche during multistage carcinogenesis. Nat Rev Cancer 2013;13:511–8.
9. Plaks V, Kong N, Werb Z. The cancer stem cell niche: how essential is the niche in regulating stemness of tumor cells? Cell Stem Cell 2015;16:225–38.
10. Calabrese C, Poppleton H, Kocak M, Hogg TL, Fuller C, Hamner B, et al. A perivascular niche for brain tumor stem cells. Cancer Cell 2007;11:69–82.
11. Beck B, Driessens G, Goossens S, Youssef KK, Kuchnio A, Caauwe A, et al. A vascular niche and a VEGF-Nrp1 loop regulate the initiation and stemness of skin tumours. Nature 2011;478:399–403.
12. Quante M, Tu SP, Tomita H, Gonda T, Wang SSW, Takashi S, et al. Bone marrow-derived myofibroblasts contribute to the mesenchymal stem cell niche and promote tumor growth. Cancer Cell 2011;19:257–72.
13. Li HJ, Reinhardt F, Herschman HR, Weinberg RA. Cancer-stimulated mesenchymal stem cells create a carcinoma stem cell niche via prostaglandin E2 signaling. Cancer Discov 2012;2:840–55.
14. Liu S, Ginestier C, Ou SJ, Clouthier SG, Patel SH, Monville F, et al. Breast cancer stem cells are regulated by mesenchymal stem cells through cytokine networks. Cancer Res 2011;71:614–24.
15. Yamamoto M, Taguchi Y, Ito-Kureha T, Semba K, Yamaguchi N, Inoue J. NF- κB non-cell-autonomously regulates cancer stem cell populations in the basal- like breast cancer subtype. Nat Commun 2013;4:2299.
16. Lu H, Clauser KR, Tam WL, Fröse J, Ye X, Eaton EN, et al. A breast cancer stem cell niche supported by juxtacrine signalling from monocytes and macrophages. Nat Cell Biol 2014;16:1105–17.
17. Orimo A, Gupta PB, Sgroi DC, Arenzana-Seisdedos F, Delaunay T, Naeem R, et al. Stromal fibroblasts present in invasive human breast carcinomas promote tumor growth and angiogenesis through elevated SDF-1/CXCL12 secretion. Cell 2005;121:335–48.
18. Hu M, Yao J, Carroll DK, Weremowicz S, Chen H, Carrasco D, et al. Regulation of in situ to invasive breast carcinoma transition. Cancer Cell 2008;13:394–406.
19. Malanchi I, Santamaria-Martínez A, Susanto E, Peng H, Lehr HA, Delaloye JF, et al. Interactions between cancer stem cells and their niche govern metastatic colonization. Nature 2012;481:85–9.
20. Orimo A, Weinberg RA. Stromal fibroblasts in cancer: a novel tumor-promoting cell type. Cell Cycle 2006;5:1597–601.
21. Kalluri R, Zeisberg M. Fibroblasts in cancer. Nat Rev Cancer 2006;6:392–401.

22. Vermeulen L, De Sousa EMelo F, van der Heijden M, Cameron K, de Jong JH, Borovski T, et al. Wnt activity defines colon cancer stem cells and is regulated by the microenvironment. Nat Cell Biol 2010;12:468–76.
23. Lotti F, Jarrar AM, Pai RK, Hitomi M, Lathia J, Mace A, et al. Chemotherapy activates cancer-associated fibroblasts to maintain colorectal cancer-initiating cells by IL-17A. J Exp Med 2013;210:2851–72.
24. Chen WJ, Ho CC, Chang YL, Chen HY, Lin CA, Ling TY, et al. Cancer-associated fibroblasts regulate the plasticity of lung cancer stemness via paracrine signalling. Nat Commun 2014;5:3472.
25. Holland JD, Györffy B, Vogel R, Eckert K, Valenti G, Fang L, et al. Combined Wnt/β-catenin, Met, and CXCL12/CXCR4 signals characterize basal breast cancer and predict disease outcome. Cell Rep 2013;5:1214–27.
26. Sugimoto H, Mundel TM, Kieran MW, Kalluri R. Identification of fibroblast heterogeneity in the tumor microenvironment. Cancer Biol Ther 2006;5:1640–6.
27. Erez N, Truitt M, Olson P, Arron ST, Hanahan D. Cancer-associated fibroblasts are activated in incipient neoplasia to orchestrate tumor-promoting inflammation in an NF-kappaB-dependent manner. Cancer Cell 2010;17:135–47.
28. Dontu G, Abdallah WM, Foley JM, Jackson KW, Clarke MF, Kawamura MJ, et al. In vitro propagation and transcriptional profiling of human mammary stem/progenitor cells. Genes Dev 2003;17:1253–70.
29. Ponti D, Costa A, Zaffaroni N, Pratesi G, Petrangolini G, Coradini D, et al. Isolation and in vitro propagation of tumorigenic breast cancer cells with stem/progenitor cell properties. Cancer Res 2005;65:5506–11.
30. Debnath J, Brugge JS. Modelling glandular epithelial cancers in three-dimensional cultures. Nat Rev Cancer 2005;5:675–88.
31. Vargo-Gogola T, Rosen JM. Modelling breast cancer: one size does not fit all. Nat Rev Cancer 2007;7:659–72.
32. Huang DW, Sherman BT, Tan Q, Kir J, Liu D, Bryant D, et al. DAVID Bioinformatics Resources: expanded annotation database and novel algorithms to better extract biology from large gene lists. Nucleic Acids Res 2007;35:W169–75.
33. Yauch RL, Gould SE, Scales SJ, Tang T, Tian H, Ahn CP, et al. A paracrine requirement for hedgehog signalling in cancer. Nature 2008;455:406–10.
34. Mak KK, Bi Y, Wan C, Chuang PT, Clemens T, Young M, et al. Hedgehog signaling in mature osteoblasts regulates bone formation and resorption by controlling PTHrP and RANKL expression. Dev Cell 2008;14:674–88.
35. Varjosalo M, Taipale J. Hedgehog: functions and mechanisms. Genes Dev 2008;22:2454–72.
36. Subramanian A, Tamayo P, Mootha VK, Mukherjee S, Ebert BL, Gillette MA, et al. Gene set enrichment analysis: a knowledge-based approach for interpreting genome-wide expression profiles. Proc Natl Acad Sci U S A 2005;102:15545–50.
37. Rhodes DR, Yu J, Shanker K, Deshpande N, Varambally R, Ghosh D, et al. ONCOMINE: a cancer microarray database and integrated data-mining platform. Neoplasia 2004;6:1–6.
38. Finak G, Bertos N, Pepin F, Sadekova S, Souleimanova M, Zhao H, et al. Stromal gene expression predicts clinical outcome in breast cancer. Nat Med 2008;14:518–27.
39. Spike BT, Engle DD, Lin JC, Cheung SK, La J, Wahl GM. A mammary stem cell population identified and characterized in late embryogenesis reveals similarities to human breast cancer. Cell Stem Cell 2012;10:183–97.
40. Choi H, Sheng J, Gao D, Li F, Durrans A, Ryu S, et al. Transcriptome analysis of individual stromal cell populations identifies stroma-tumor crosstalk in mouse lung cancer model. Cell Rep 2015;10:1187–201.
41. Ingham PW, McMahon AP. Hedgehog signaling in animal development: paradigms and principles. Genes Dev 2001;15:3059–87.
42. Rudin CM, Hann CL, Laterra J, Yauch RL, Callahan CA, Fu L, et al. Treatment of medulloblastoma with hedgehog pathway inhibitor GDC-0449. N Engl J Med 2009;361:1173–8.
43. Sekulic A, Migden MR, Oro AE, Dirix L, Lewis KD, Hainsworth JD, et al. Efficacy and safety of vismodegib in advanced basal-cell carcinoma. N Engl J Med 2012;366:2171–9.
44. Kasper M, Jaks V, Fiaschi M, Toftgård R. Hedgehog signalling in breast cancer. Carcinogenesis 2009;30:903–11.
45. Bailey JM, Swanson BJ, Hamada T, Eggers JP, Singh PK, Caffery T, et al. Sonic hedgehog promotes desmoplasia in pancreatic cancer. Clin Cancer Res 2008;14:5995–6004.
46. Mukherjee S, Frolova N, Sadlonova A, Novak Z, Steg A, Page GP, et al. Hedgehog signaling and response to cyclopamine differ in epithelial and stromal cells in benign breast and breast cancer. Cancer Biol Ther 2006;5:674–83.
47. O'Toole SA, Machalek DA, Shearer RF, Millar EKA, Nair R, Schofield P, et al. Hedgehog overexpression is associated with stromal interactions and predicts for poor outcome in breast cancer. Cancer Res 2011;71:4002–14.
48. Teissedre B, Pinderhughes A, Incassati A, Hatsell SJ, Hiremath M, Cowin P. MMTV-Wnt1 and -DeltaN89beta-catenin induce canonical signaling in distinct progenitors and differentially activate Hedgehog signaling within mammary tumors. PLoS ONE 2009;4:e4537.
49. Tsuyada A, Chow A, Wu J, Somlo G, Chu P, Loera S, et al. CCL2 mediates cross-talk between cancer cells and stromal fibroblasts that regulates breast cancer stem cells. Cancer Res 2012;72:2768–79.
50. Hermann PC, Huber SL, Herrler T, Aicher A, Ellwart JW, Guba M, et al. Distinct populations of cancer stem cells determine tumor growth and metastatic activity in human pancreatic cancer. Cell Stem Cell 2007;1:313–23.